Available online at www.sciencedirect.com
ScienceDirect
European Journal of Mechanics B/Fluids 25 (2006) 877–893

Method of fundamental solutions for multidimensional Stokes equations by the dual-potential formulation

D.L. Young [a,*], C.L. Chiu [a], C.M. Fan [a], C.C. Tsai [b], Y.C. Lin [a]

[a] *Department of Civil Engineering & Hydrotech Research Institute, National Taiwan University, Taipei, Taiwan*
[b] *Department of Information Technology, Toko University, Chia-Yi County, Taiwan*

Received 25 August 2005; received in revised form 22 February 2006; accepted 23 February 2006

Available online 16 May 2006

Abstract

A simple and accurate boundary-type meshless method of fundamental solutions (MFS) is applied to solve both 2D and 3D Stokes flows based on the dual-potential formulation of velocity potential and stream function vector. Using the dual-potential concept, the solutions of both 2D and 3D Stokes flows are obtained by combining the much simpler fundamental solutions of Laplace (potential) and bi-harmonic equations without using the complicated singular fundamental solutions such as Stokeslets and their derivatives as well as source doublet hypersingularity. The developed algorithm is used to test five numerical experiments for 2D flows: (1) circular cavity, (2) wave-shaped bottom cavity and (3) circular cavity with eccentric rotating cylinder; and for 3D flows: (4) a uniform flow passing a sphere and (5) a uniform flow passing a pair of spheres. Good results are obtained as comparing with solutions of analytical and numerical methods such as FEM, BEM and other meshfree schemes.

Keywords: Method of fundamental solutions; Dual-potential formulation; Velocity potential and stream function vector; 2D and 3D Stokes flows; Laplace equation; Bi-harmonic equation

1. Introduction

In the fluid mechanics literature there are three major formulations for the dependent variables to solve the multidimensional Navier–Stokes or the much simpler Stokes equations. They are (1) primitive variables of velocity–pressure, (2) velocity–vorticity and (3) vorticity–potential forms. Each formulation will suffer different degrees of difficulty in imposing the boundary conditions. In this study we only consider Stokes equations by neglecting the non-linear convective term to form the creeping flows through a novel dual-potential formulation of the velocity potential and stream function vector. Stokes flows are classical problems in computational fluid dynamics (CFD), and have ubiquitous applications in many interdisciplinary fields.

For illustrations, in the primitive variables of velocity–pressure formulation: Abousleiman and Cheng [1] solved the 2D internal flows using the boundary element method (BEM) based on the Stokeslets, and Zeb et al. [2] also applied the same BEM to analyze 2D flows with more general boundary conditions and arbitrary geometries. Alves

* Corresponding author. Tel.: +886 2 23626114; fax: +886 2 23626114.
E-mail address: dlyoung@ntu.edu.tw (D.L. Young).

0997-7546/$ – see front matter
doi:10.1016/j.euromechflu.2006.02.004

and Silvestre [3], Young et al. [4,5] and Chen et al. [6] solved 2D and 3D interior problems by the MFS based on the Stokeslets, while Tsai et al. [7] used the same concept to study 3D exterior flows. In the velocity–vorticity formulation: Fan and Young [8] applied the non-singular BEM to solve the 2D flows. Young et al. [9] used the meshless multiquadrics method to solve 2D and 3D flows. Tsai et al. [10] used the MFS along with the dual reciprocity method (DRM), called meshless BEM, to solve the 3D interior and exterior flows. As far as applications of vorticity–potential approach for Stokes flows are concerned, in 2D flows, the Stokes equations may be transformed to the vorticity–stream function form governed by the Laplace and Poisson equations or even only the bi-harmonic stream function equation. Fairweather, Karageorghis and coworkers [11–13] used the MFS based on the formulation of bi-harmonic stream function to analyze 2D flows. However it is not straightforward to extend 2D stream function formulation to 3D flows, and even it becomes a controversial issue in the realm of CFD [14].

A general formulation by the dual-potential of velocity potential and stream function vector for both 2D and 3D Stokes equations is developed in this study. Comparing with the traditional stream function approach, the proposed scheme can be easily extended from 2D to 3D problems and to the fluids with dilatation. The Helmholtz decomposition theorem is used to segregate the Stokes flow into the sum of a potential flow and a viscous flow, so that the fundamental solutions of Stokes equations can be transformed from the complicated Stokeslets [15] to the combination of the much simpler fundamental solutions of Laplace equation for velocity potential and bi-harmonic equations for stream function vector (dual-potential method) following the lead of Hirasaki and Hellums [16]. In primitive variable formulation the decomposition of the Stokes flow into the sum of a potential flow and a viscous flow was originally studied by Chwang and Wu [17] and also followed by Dabros [18] by using the singularity method. However, much sophisticated singular fundamental solutions such as Stokeslets and the derivatives as well as hypersingularity of source doublet were employed in Chwang and Wu and Dabros works. Another rationale to use the proposed method lies in the very simple imposition of the boundary conditions of this dual-potential formulation. In this study the boundary conditions for both the velocity potential and stream function vector are simultaneously considered by specifying the no-slip boundary conditions according to special properties of the MFS, which otherwise is rather difficult to satisfy by other numerical methods such as the advanced works of [14,16]. Once the unknown coefficients are determined from the imposed velocity boundary conditions, the distributions of velocity and vorticity over the entire computational domain can be directly evaluated. Comparing with other formulations such as the velocity–vorticity and vorticity–potential, in 3D problems the number of variables in the present scheme has been reduced from six to only four for both formulations, and in 2D problems it is only two instead of three for the velocity–vorticity formulation. The reduction of number of variables can decrease the computational time and required storage. Meanwhile in the velocity–vorticity and vorticity–potential formulations, the treatment of non-homogeneous source term is inevitable in the numerical procedure due to the existence of the Poisson equations of both forms. A significance to note is that the algorithm developed in this study is a purely boundary-type meshless method of MFS, particularly suitable for exterior problems. In other words, no artificial far field boundaries are required in the MFS formulation.

The MFS was first proposed by Kupradze and Aleksidze [19]. Recently, the MFS has been widely used in the numerical solutions of Poisson equations [20,21], diffusion equations [22,23], Helmholtz equations [24,25], modified Helmholtz equations [10,22], bi-harmonic equations [11–13] and Stokes equations [3–7,10–13], etc. The implementations of MFS were also discussed in the references of [26–28]. Good reviews on the advances on the MFS can be referred to the literature of [29–31]. The MFS can be exceedingly effective for solving inverse or degenerate problems in which missing or degenerate boundary data or the solutions at a few points within the domain are required, such as the inverse Stokes and degenerate Eigenanalysis problems [6,32]. Using some simplifying assumptions and mathematical manipulations, it can be shown that the MFS is equivalent to the indirect BEM [19,30]. In addition, the meshless MFS can get rid of the mesh generation and the numerical integration. Thus the MFS is much easier to implement than the indirect BEM, as far as numerical algorithm is concerned.

Both the BEM and MFS are based on the fundamental solutions of the governing equations, and their solution methodologies do not depend on the discretization of interior computational regions. However, unlike the singular integrals of BEM, the basic concept of the MFS is to decompose the solutions of the partial differential equations by superposition of the fundamental solutions with proper intensities. Wherein, the unknown coefficients can be obtained by the collocations of the boundary conditions. Since the MFS locates the source points outside the computational domain, no special treatments for the singularities of fundamental solutions are required. Therefore, the MFS is considered to be a grid-free scheme which depends only upon distances between pair of points of the so-called radial basis functions, thus MFS is more suitable for the exterior and irregular domain problems.

The aim of this paper is to use a simple, accurate and meshless MFS to solve 2D and 3D Stokes problems based on the combination of the Laplace equation for velocity potential and vector bi-harmonic equation for stream function vector by using the Helmholtz decomposition theorem. The following five numerical examples are considered to demonstrate the accuracy and feasibility of the proposed numerical method: for 2D flows: (1) circular cavity, (2) wave-shaped bottom cavity and (3) circular cavity with eccentric rotating cylinder, and for 3D flows: (4) a uniform flow passing a sphere and (5) a uniform flow passing a pair of spheres. Comparisons of present results with the solutions of analytical and other numerical methods such as BEM, FEM as well as MFS based on the Stokeslets and velocity–vorticity forms will be carried out to confirm the simplicity and accuracy of the proposed scheme.

2. Governing equations

The equations for incompressible steady-state Stokes problems are governed by the conservations of mass and momentum:

Continuity equation:

$$\nabla \cdot \vec{u} = 0. \tag{1}$$

Momentum equation:

$$0 = -\nabla p + \mu \nabla^2 \vec{u}. \tag{2}$$

Subjected to the following no-slip boundary conditions:

$$\vec{u} = \vec{U} \tag{3}$$

where $\vec{u} = (u, v, w)$ is the velocity vector; p is the pressure; μ is the dynamic viscosity; $\vec{U}$ is known a priori boundary velocity. Eqs. (1), (2) and (3) constitute the so called primitive variables of velocity–pressure formulation. By definition, the vorticity vector $\vec{\omega} = (\xi, \eta, \zeta)$ is expressed as:

$$\vec{\omega} = \nabla \times \vec{u}. \tag{4}$$

Taking the curl to Eq. (2) with constant μ, and using Eq. (4), we obtain the steady-state vorticity transport equation for Stokes flows as follows:

$$\nabla^2 \vec{\omega} = 0. \tag{5}$$

Taking the curl to Eq. (4) and using Eq. (1), we get

$$\nabla^2 \vec{u} = -\nabla \times \vec{\omega}. \tag{6}$$

Eqs. (5) and (6) are the governing equations for steady-state Stokes flows in another form known as the velocity–vorticity formulation.

The Helmholtz decomposition theorem [16,33,34] states that any vector $\vec{u}$ can be written as the sum of two parts, one is curl-free and the other is solenoidal. In flow fields, the velocity is thereby decomposed into a potential flow and a viscous flow. In other words, the velocity $\vec{u}$ can be decomposed into the following form:

$$\vec{u} = -\nabla \phi + \nabla \times \vec{\psi}. \tag{7}$$

Substituting the above equation into Eq. (1), we obtain the Laplace equation for the velocity potential, ϕ:

$$\nabla^2 \phi = 0. \tag{8}$$

Substituting Eq. (7) into Eq. (4) and following [16,35]

$$\nabla \cdot \vec{\psi} = 0. \tag{9}$$

We obtain

$$\nabla^2 \vec{\psi} = -\vec{\omega}. \tag{10}$$

It is noted that adoption of Eqs. (1), (5) and (10) is the conventional vorticity–potential formulation and reduces to the vorticity–stream function form in 2D flows. However, the present dual-potential formulation is easier to extend

to fluids with dilatation such as incompressible flows with source terms or unsteady compressible flows; if Eq. (8) is modified by the Poisson equation. From Eqs. (5) and (10), we finally obtain the vector bi-harmonic equation for stream function vector, $\vec{\psi} = (\psi_1, \psi_2, \psi_3)$:

$$\nabla^2 \nabla^2 \vec{\psi} = 0. \tag{11}$$

From the above deduction it is remarked that the velocity $\vec{u}$ is written as two parts in the form given in Eq. (7) by the Helmholtz decomposition theorem. As a result, ϕ and $\vec{\psi}$ can be obtained respectively by the MFS from the Laplace equation, Eq. (8), and vector bi-harmonic equation, Eq. (11). However, we choose not to solve for ϕ and $\vec{\psi}$ separately and directly. Instead we select to determine $\vec{u}$ explicitly from Eq. (7) due to the convenience of imposing no-slip boundary conditions of Eq. (3) and the unique merits of the MFS (the MFS solutions behave like semi-analytical solutions so that it is very easy to differentiate ϕ and $\vec{\psi}$), as it will be explained in the following section. This is quite different from the traditional ways to directly impose the boundary conditions on ϕ and $\vec{\psi}$, because their boundary conditions cannot be imposed in an easy way [16]. Since our main interests are in the velocity fields, in this study we do not need to explicitly know those ϕ and $\vec{\psi}$ boundary conditions and thus only velocity boundary conditions are required as we can make use of Eq. (7). Eqs. (8), (11) and (7) thus constitute the governing equations of velocity field and Eq. (3) is the well-posed velocity boundary condition using the dual-potential formulation of velocity potential and stream function vector for 2D and 3D Stokes equations.

3. Formulation of the Method of Fundamental Solutions (MFS)

The fundamental solution, also known as the free space Green's function, is defined by

$$\mathfrak{L} G(\vec{x}; \vec{x}_0) = -\delta(\vec{x} - \vec{x}_0) \tag{12}$$

where $\mathfrak{L}$ is a linear spatial differential operator, $\delta(\vec{x} - \vec{x}_0)$ is the well-known Dirac delta function, $\vec{x} = (x, y, z)$ is the position of the field point, $\vec{x}_0 = (x_0, y_0, z_0)$ is the location of the source point, and the distance between a field point and a source point is defined by $r = |\vec{x} - \vec{x}_0|$.

By applying Fourier transform theory to Eq. (12), the fundamental solution of the 2D Laplace equation is obtained as

$$G_\phi(\vec{x}; \vec{x}_0) = \frac{-1}{2\pi} \ln r. \tag{13}$$

Similarly, the fundamental solution for the 2D bi-harmonic equation can be written as

$$G_\psi(\vec{x}; \vec{x}_0) = \frac{-1}{8\pi} r^2 \ln r. \tag{14}$$

The principle of superposition is employed for linear governing equations. Therefore in the spirit of MFS formulation the solution is represented by a series of fundamental solutions with singularities located outside the computational domain. The unknown coefficients of the series of fundamental solutions are regarded as the strengths of corresponding fundamental solutions. Therefore the discretizations of stream function ψ and velocity potential ϕ are performed and represented as:

$$\psi(\vec{x}_i) = \sum_{j=1}^{N} \big[\alpha_j G_\psi(\vec{x}_i; \vec{x}_{0j})\big], \tag{15}$$

$$\phi(\vec{x}_i) = \sum_{j=1}^{N} \big[\beta_j G_\phi(\vec{x}_i; \vec{x}_{0j})\big] \tag{16}$$

where $\vec{x}_i$ is the i-th field point, $\vec{x}_{0j}$ is the j-th source point, N is the number of the source points and α_j and β_j, the unknown coefficients, are respectively associated with the fundamental solutions of stream function and velocity potential. Therefore, the velocity field $\vec{u} = (u, v, 0)$ is represented by using Eq. (7) as:

$$u(\vec{x}_i) = \sum_{j=1}^{N}\left[\alpha_j(1+2\ln r_{ij})(y_i - y_{0j})\right] + \sum_{j=1}^{N}\left[\beta_j \frac{x_i - x_{0j}}{r_{ij}^2}\right], \tag{17a}$$

$$v(\vec{x}_i) = -\sum_{j=1}^{N}\left[\alpha_j(1+2\ln r_{ij})(x_i - x_{0j})\right] + \sum_{j=1}^{N}\left[\beta_j \frac{y_i - y_{0j}}{r_{ij}^2}\right] \tag{17b}$$

where $r_{ij} = |\vec{x}_i - \vec{x}_{0j}|$.

The boundary conditions of velocity components of Eq. (3) are then collocated to find the unknown coefficients. This results in a $2N \times 2N$ linear system. After the $2N$ unknown coefficients of α_j and β_j are determined, we obtain the velocity first and then the vorticity fields. The vorticity field $\vec{\omega} = (0, 0, \zeta)$ for 2D Stokes flow is shown as:

$$\zeta(\vec{x}_i) = -\sum_{j=1}^{N}\left[\alpha_j(4+4\ln r_{ij})\right]. \tag{18}$$

Though the bi-harmonic equation of stream function can be employed to solve the 2D Stokes flows as it has been done by Fairweather, Karageorghis and collaborators [11–13], inhere we do not directly find the stream function but only take the curl of the stream function to impose the no-slip boundary conditions. The imposition of the boundary conditions for the bi-harmonic equation for the stream function only as performed in [11–13] is more complicated and involved than the present method, since higher order boundary conditions are necessary if the stream function should be found directly. This implies that two terms (one augmented term like $\ln r$ in the 2D case) of the fundamental solution of the bi-harmonic equation are necessary instead like present model no augmented term is needed.

We next consider the numerical formulations for 3D problems. The fundamental solutions for the 3D Laplace and bi-harmonic equations are:

$$G_\phi(\vec{x}; \vec{x}_0) = \frac{1}{4\pi r}, \tag{19}$$

$$G_\psi(\vec{x}; \vec{x}_0) = \frac{1}{4\pi} r. \tag{20}$$

Similarly, the discretizations of stream function vector $\vec{\psi} = (\psi_1, \psi_2, \psi_3)$ and velocity potential ϕ are given as:

$$\psi_1(\vec{x}_i) = \sum_{j=1}^{N}\left[\alpha_j^1 G_\psi(\vec{x}_i; \vec{x}_{0j})\right], \tag{21a}$$

$$\psi_2(\vec{x}_i) = \sum_{j=1}^{N}\left[\alpha_j^2 G_\psi(\vec{x}_i; \vec{x}_{0j})\right], \tag{21b}$$

$$\psi_3(\vec{x}_i) = \sum_{j=1}^{N}\left[\alpha_j^3 G_\psi(\vec{x}_i; \vec{x}_{0j})\right], \tag{21c}$$

$$\phi(\vec{x}_i) = \sum_{j=1}^{N}\left[\beta_j G_\phi(\vec{x}_i; \vec{x}_{0j})\right]. \tag{22}$$

The velocity $\vec{u} = (u, v, w)$ for 3D problems is thus given as:

$$u(\vec{x}_i) = \sum_{j=1}^{N}\left[\alpha_j^3 \frac{y_i - y_{0j}}{r_{ij}}\right] - \sum_{j=1}^{N}\left[\alpha_j^2 \frac{z_i - z_{0j}}{r_{ij}}\right] + \sum_{j=1}^{N}\left[\beta_j \frac{-(x_i - x_{0j})}{r_{ij}^3}\right], \tag{23a}$$

$$v(\vec{x}_i) = \sum_{j=1}^{N}\left[\alpha_j^1 \frac{z_i - z_{0j}}{r_{ij}}\right] - \sum_{j=1}^{N}\left[\alpha_j^3 \frac{x_i - x_{0j}}{r_{ij}}\right] + \sum_{j=1}^{N}\left[\beta_j \frac{-(y_i - y_{0j})}{r_{ij}^3}\right], \tag{23b}$$

$$w(\vec{x}_i) = \sum_{j=1}^{N}\left[\alpha_j^2 \frac{x_i - x_{0j}}{r_{ij}}\right] - \sum_{j=1}^{N}\left[\alpha_j^1 \frac{y_i - y_{0j}}{r_{ij}}\right] + \sum_{j=1}^{N}\left[\beta_j \frac{-(z_i - z_{0j})}{r_{ij}^3}\right]. \tag{23c}$$

Meanwhile, one more compatibility equation is required to obtain the unique solutions of velocity field in 3D flows as proved by Weinan and Liu [36]. Thus, we choose to use Eq. (9) as follows:

$$\nabla \cdot \vec{\psi} = 0 = \sum_{j=1}^{N} \left[\alpha_j^1 \frac{x_i - x_{0j}}{r_{ij}} + \alpha_j^2 \frac{y_i - y_{0j}}{r_{ij}} + \alpha_j^3 \frac{z_i - z_{0j}}{r_{ij}} \right]. \tag{24}$$

A $4N \times 4N$ linear system is formed similar to the 2D flow system. After imposing the no-slip boundary conditions, we then obtain the velocity field from Eq. (23). Once the velocity is determined, we have the vorticity vector $\vec{\omega} = (\xi, \eta, \zeta)$ for 3D problems as:

$$\xi(\vec{x}_i) = \sum_{j=1}^{N} \left[\alpha_j^1 \frac{1}{r_{ij}} \right], \tag{25a}$$

$$\eta(\vec{x}_i) = \sum_{j=1}^{N} \left[\alpha_j^2 \frac{1}{r_{ij}} \right], \tag{25b}$$

$$\zeta(\vec{x}_i) = \sum_{j=1}^{N} \left[\alpha_j^3 \frac{1}{r_{ij}} \right]. \tag{25c}$$

It is worthwhile mentioning that the proposed solution algorithms of velocity field using Eq. (17) for 2D and Eq. (23) for 3D flows are much simpler than using the MFS based on the Stokeslet singularities such as cited in the references of [3–7] or the singularity methods [17,18]. This is the major reason why the proposed method is able to render a simple and accurate scheme which will be further discussed in Section 4 of the model verifications and applications.

The numerical procedures proposed in this study can be implemented by the following steps:

1. Place the distribution of field points on the boundary and select the same number of source points close to the boundary as that will be explained exclusively by numerical examples in the next section. More details about the locations of the source points can also be obtained from the references [4–6,28,32]. ($\vec{x}_s = \vec{x}_b + b(\vec{x}_b - \vec{x}_c)$; where $\vec{x}_s$, $\vec{x}_b$ and $\vec{x}_c$ are the position of the source point, boundary point and geometric center, as well as b is a free parameter.)
2. Apply Eqs. (17a), (17b) for 2D flows and Eqs. (23a)–(23c) and (24) for 3D flows to form the solution matrices, in which the coefficients α_j and β_j are regarded as the unknown variables in 2D flows, and $\alpha_j^1, \alpha_j^2, \alpha_j^3$ and β_j are the unknown variables in 3D flows.
3. Impose the boundary conditions for velocities to solve the solution matrices and obtain the unknown coefficients in the selected number of source points.
4. Evaluate the velocity and vorticity fields in the computational domain by means of summation over the source points using Eqs. (17a), (17b) and (18) for 2D flows; or Eqs. (23a)–(23c) and Eqs. (25a)–(25c) for 3D flows.

4. Model verifications and applications

4.1. Model verifications

For verification purposes we choose two benchmark problems from 2D and 3D flows, all with known exact solutions. We take a circular lid-driven cavity in 2D flow and a uniform flow passing a sphere in 3D flow.

4.1.1. A circular cavity

To verify the capability of our numerical algorithm, the lid-driven Stokes flow in a circular cavity is considered. The upper half surface of the circular cavity moves with a constant unit circumferential velocity in the counterclockwise direction and no-slip boundary conditions are imposed on the lower half surface of the circular cavity. Fig. 1 depicts the sketched geometric configuration and boundary conditions and also the distribution of source and field points. This

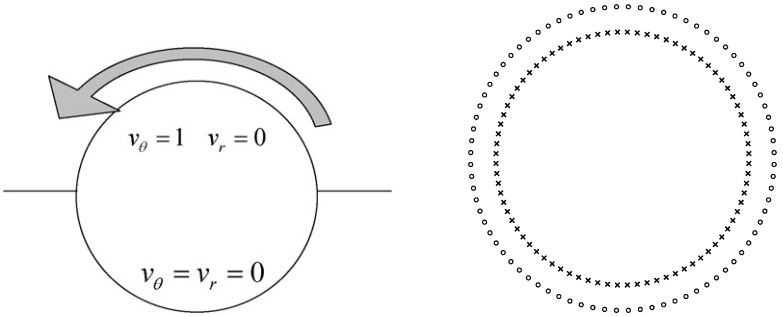

Fig. 1. (a) Schematic diagram of a circular cavity. (b) Distribution of the source (○) and field (×) points.

Table 1
RMSE of u-velocity for different source points at $b = 0.2$ in the example 4.1.1

N	80	120	160	200
RMSE	1.49×10^{-3}	1.82×10^{-5}	1.13×10^{-5}	6.93×10^{-6}

Table 2
RMSE of u-velocity for different locations of source points with $N = 200$ in the example 4.1.1

b	0.08	0.12	0.16	0.20
RMSE	6.84×10^{-6}	6.93×10^{-6}	6.93×10^{-6}	6.93×10^{-6}

popular benchmark problem is used to demonstrate that whether the algorithm is robust, and the numerical results will be compared with the analytical solutions by Hwu et al. [37].

The illustrations on the distributions of velocity vector, vorticity contour, as well as u- and v-velocity contours are shown from Figs. 2–5 respectively, which exhibit the symmetric characteristics of the flow variables as expected for the Stokes flow. All the above numerical results are implemented with 200 source points. To give a more quantitative understanding of accuracy, the root-mean-square errors (RMSE) of u-velocity at the vertical centerlines of the cavity are depicted in Tables 1 and 2, respectively. Here, the RMSE is regarded as an index for the accuracy measure and defined as follows:

$$\text{RMSE} \equiv \sqrt{\frac{\sum_{i=1}^{N} (\text{numerical result} - \text{exact solution})_i^2}{N}}. \tag{26}$$

In Table 1, the RMSE of computational results are obtained by using 80, 120, 160 and 200 source points to establish a convergent and node independent scheme. Comparing with analytical solution, the RMSE of numerical results for the source points greater than 120 are all in the order of 10E–5. Good agreement is observed even for 80 collocation nodes. The non-singular BEM (NSBEM) [8] has to use at least 400 node points to obtain the same accuracy as the present method. The RMSE of the solutions corresponding to different source locations are displayed in Table 2. It reveals that the accuracy related to the parameter "b" is not sensitive, and the farther positions of the source can get better resolution in our study range.

4.1.2. A uniform flow passing a sphere

To verify the proposed numerical method in 3D exterior domain, the problem of the uniform flow passing a sphere is taken as the second example. Fig. 6 shows the flow configuration and the distribution of source and filed points. The exterior Stokes problems are very difficult to analyze by using the domain discretization method, because of the huge computational data and the satisfaction of far field outflow boundary conditions. Unlike other domain discretization methods, the MFS inherits the great capability for such unbound region problems.

The analytical solution of the problem can be found from [38,39] as follows:

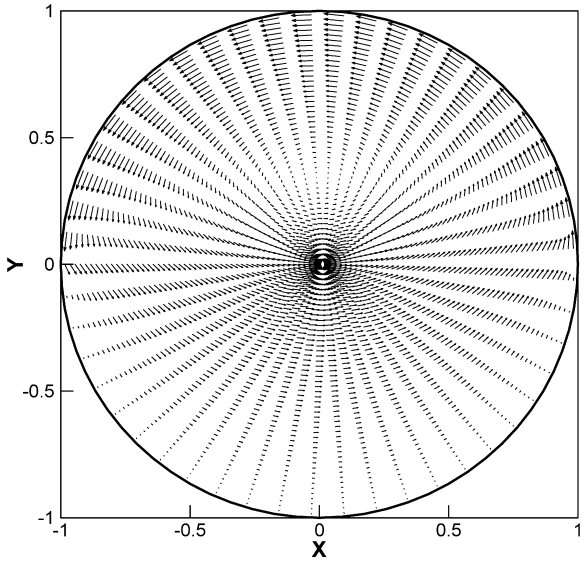

Fig. 2. Velocity vector for the Stokes flow in a circular cavity ($N = 200$).

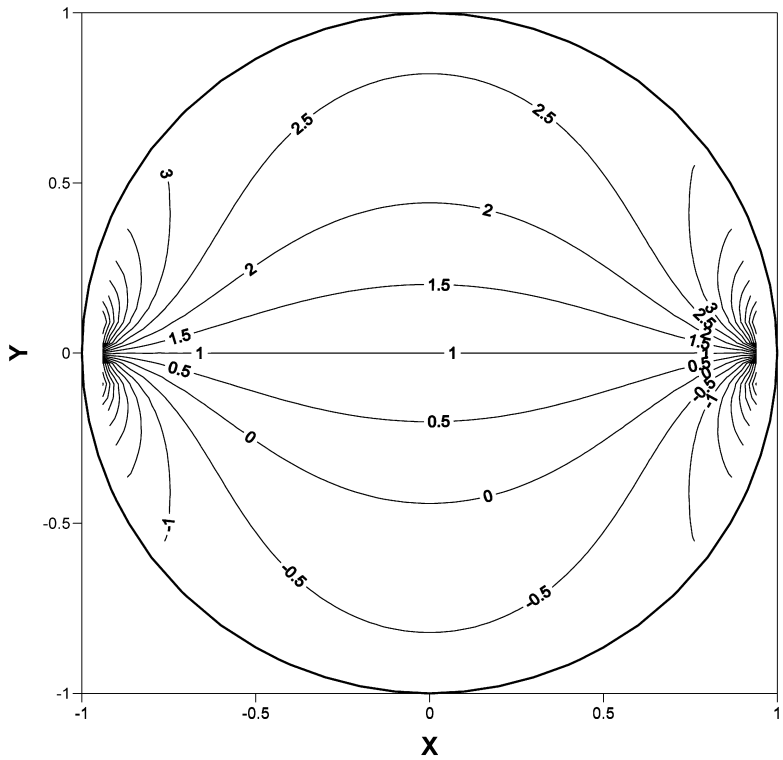

Fig. 3. Vorticity contour for the Stokes flow in a circular cavity ($N = 200$).

$$u_r = U_0 \cos\theta \left[1 - \frac{3a}{2r} + \frac{a^3}{2r^3}\right], \tag{27}$$

$$u_\theta = -U_0 \sin\theta \left[1 - \frac{3a}{4r} - \frac{a^3}{4r^3}\right] \tag{28}$$

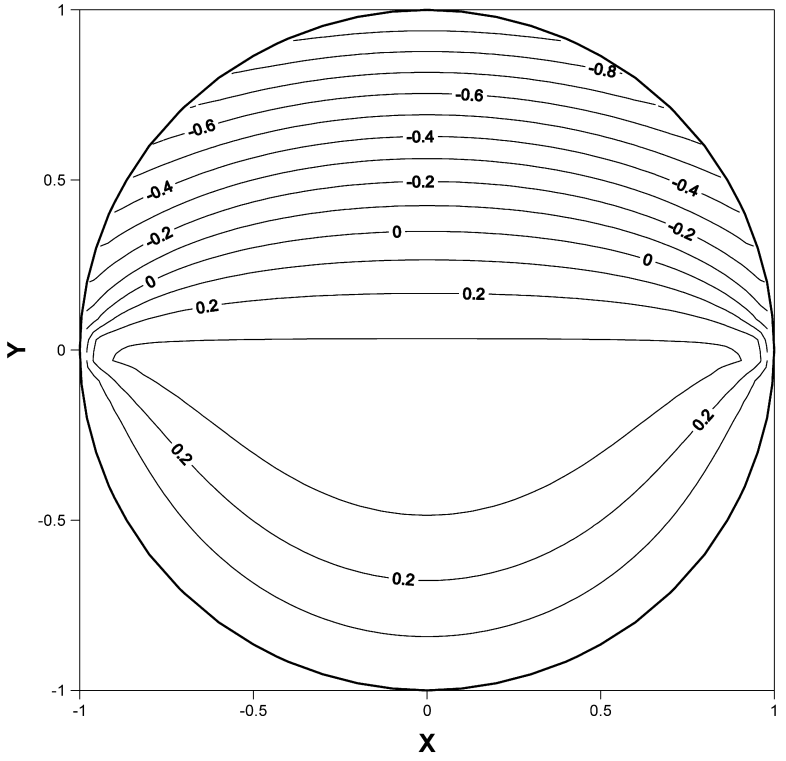

Fig. 4. u-velocity contour for the Stokes flow in a circular cavity ($N = 200$).

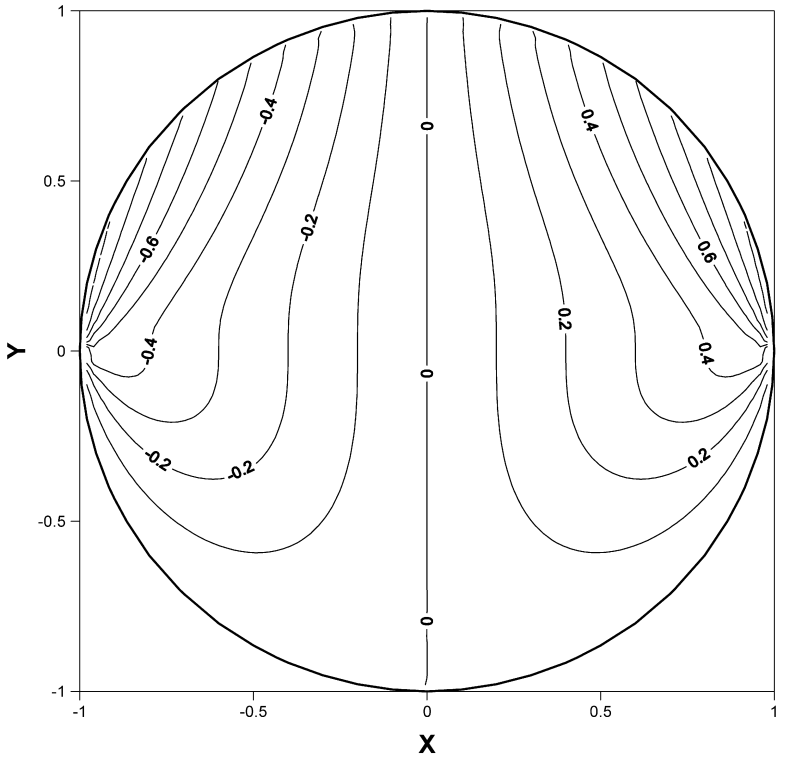

Fig. 5. v-velocity contour for the Stokes flow in a circular cavity ($N = 200$).

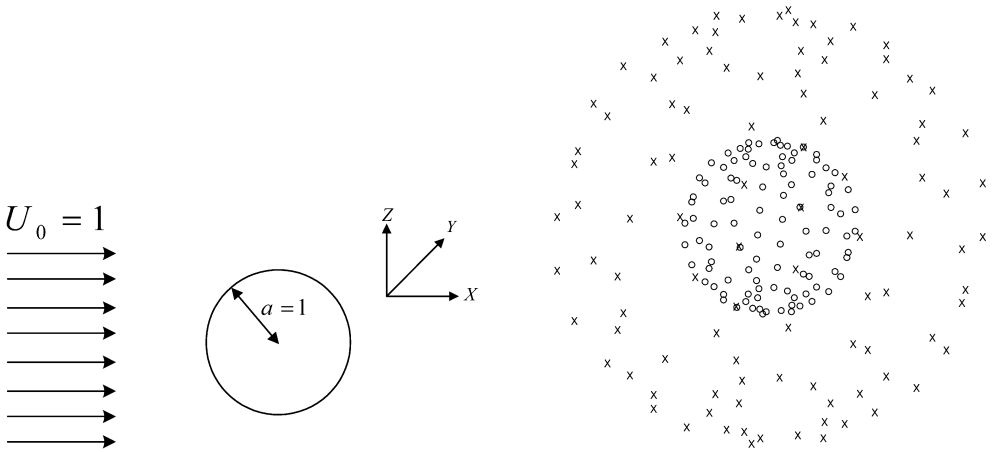

Fig. 6. (a) Flow field configuration of the uniform flow passing a sphere. (b) Distribution of the source (○) and field (×) points.

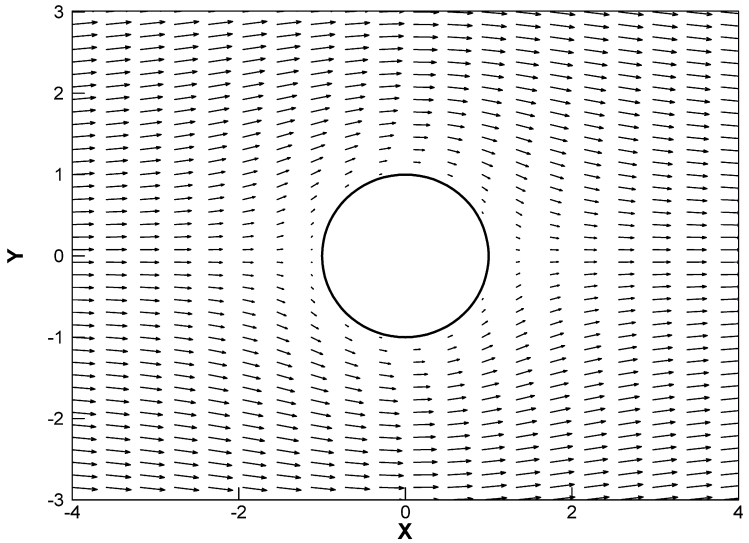

Fig. 7. Velocity vector for the Stokes flow at the plane of $z = 0$ ($N = 100$).

Table 3
RMSE of u-velocity for different source points at $b = -0.6$ in the example 4.1.2

N	49	100	256	400
RMSE	9.76×10^{-5}	1.08×10^{-5}	1.54×10^{-7}	1.46×10^{-10}

in which U_0 is the free-stream velocity, a is the radius of sphere, r and θ are the spherical coordinates with the assumption of spherical symmetry, $\partial/\partial\phi = 0$. Moreover, both U_0 and a are set to be unity in our numerical experiment, and $\theta = 0$ corresponds to the flowing away direction of the fluid.

The velocity vector field in the plane $z = 0$ by taking 100 source points is shown in Fig. 7. To achieve such an accurate measure, 266 or more node points are required in the MFS based on the formulation of Stokeslets by Tsai et al. [7]. The main reason lies in the more complicated fundamental solutions of the MFS based on the formulation of Stokeslets. A source point refinement study was performed to verify the node independence and the accuracy of the method. Table 3 depicts the comparison of the RMSE of the velocity profiles along the z direction at $x = y = 0$,

Table 4
RMSE of u-velocity for different locations of source points with $N = 400$ in the example 4.1.2

b	-0.2	-0.4	-0.6	-0.8
RMSE	7.63×10^{-5}	2.82×10^{-7}	1.46×10^{-10}	2.42×10^{-13}

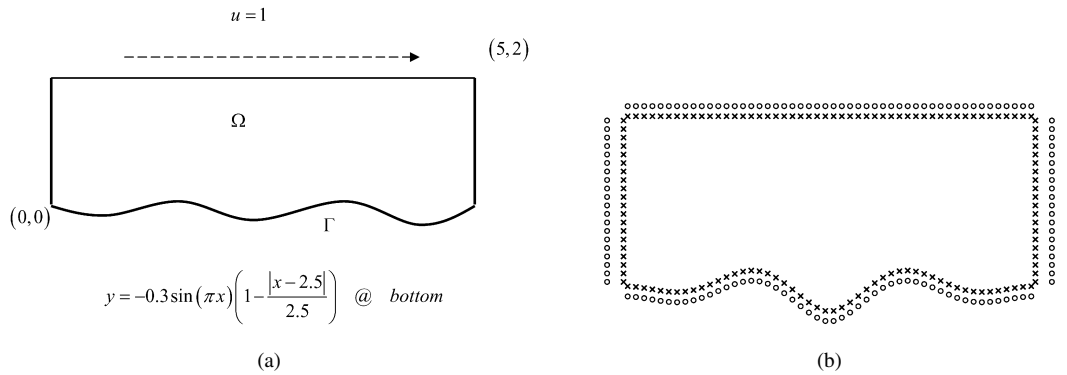

Fig. 8. (a) Schematic diagram of a wave-shaped bottom cavity. (b) Distribution of the source (○) and field (×) points.

obtained by four discretizations ranging from 49 to 400 source points. The numerical results by different collocation points show generally good agreement with the analytical solutions.

It reveals that the larger number of nodes always yields more accurate results as expected. We obtained the RMSE in the order of 10E–05 when 49 nodes are used. If 400 nodes are utilized the RMSE drops to the order of 10E-10. Even if only 49 node points are used, the results are still competitive to other numerical methods in accuracy. This is reflected from the meshless BEM [10] which requires 1,650 nodes to get the same order of accuracy since DRM was needed in the meshless BEM. Table 4 exhibits the RMSE of the numerical solutions with different source locations. The resolutions of the results remain steadfast in the range of source positions studied.

4.2. Model applications

Case studies of two more 2D and one more 3D Stokes flows are made to further exploit the robustness and feasibility of the proposed method.

4.2.1. A wave-shaped bottom cavity

To demonstrate the capability of the present algorithm for irregular computational geometry, the Stokes flow in a lid-driven cavity with wave-shaped bottom is taken as the third numerical experiment. Fig. 8 represents the schematic diagram as well as the distribution of the source and field points of a wave-shaped bottom cavity with top lid moving with a unit velocity in the x-direction. The movement of the top lid gives rise to a recirculating gyre pattern inside the cavity as shown by the velocity vector in Fig. 9. Fig. 10 also depicts the u-velocity distribution in the wave-shaped bottom cavity for the Stokes flow. Both of the above numerical results are implemented with 140 source points.

For further comparison purposes, the u-velocity distribution along the vertical central line is depicted in Fig. 11. Where the FEM results are obtained by using 1,957 grid nodes for velocity, 685 grid nodes for pressure and 1,272 T4/C3 triangular elements and the results are regarded as mesh-independent solutions. The results predicted by MFS show generally independent of node number when the number of nodes is larger than 140, and the solutions are also in close agreement with the FEM results. We also compare the present results with the MFS based on the formulation of Stokeslets by Young et al. [5]. It is found that the 560 source points are needed to get the same accuracy comparing with the present 280 points. It is thus convinced that the proposed method free from mesh generation can be applied to Stokes problems with complex geometry under easy implementation.

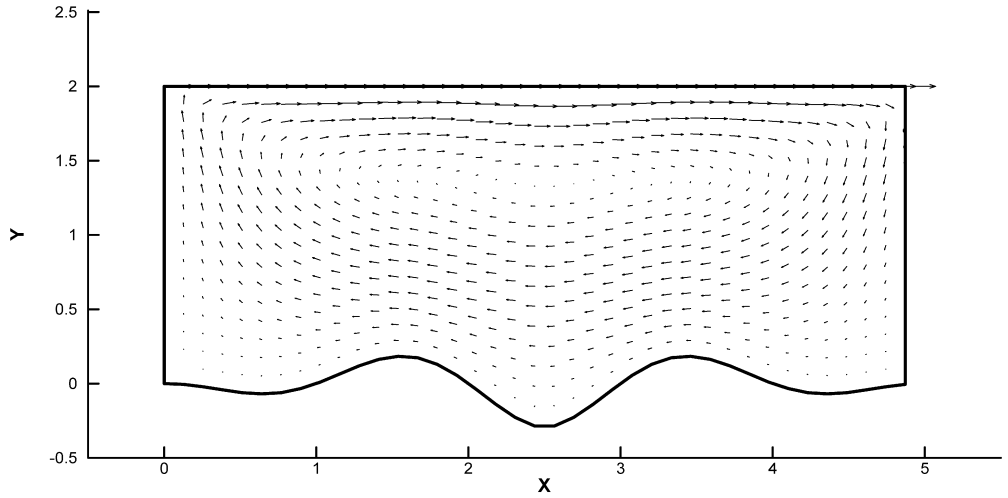

Fig. 9. Velocity vector for the Stokes flow in a wave-shaped bottom cavity ($N = 140$).

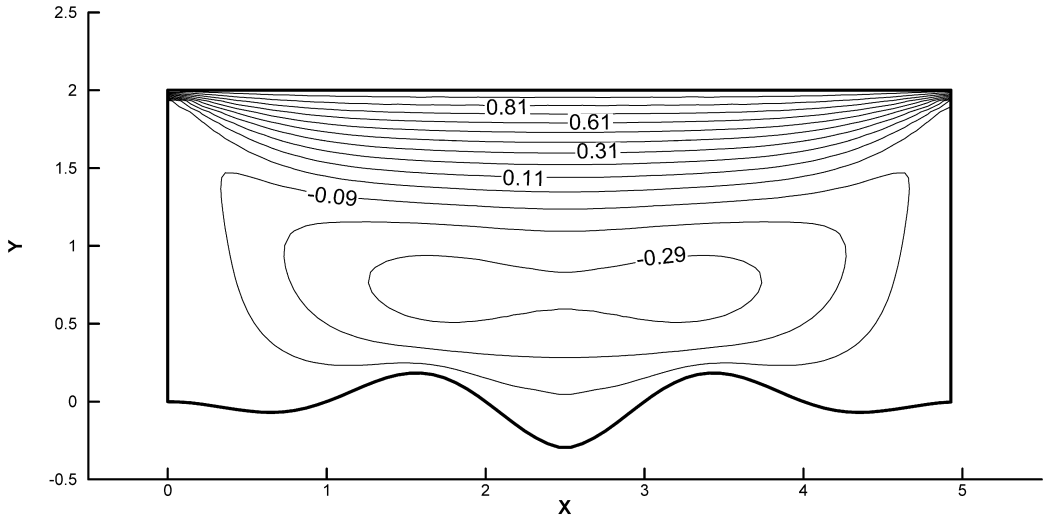

Fig. 10. u-velocity contour for the Stokes flow in a wave-shaped bottom cavity ($N = 140$).

4.2.2. A circular cavity with eccentric rotating cylinder

The presented model is carried out to solve the 2D Stokes flow confined in the two eccentric cylinders. The problem of interest is sketched in Fig. 12 including geometric configuration and the associated distributions of source and field points. The outer cylinder with radius $R_1 = 1$ centers on the original, and the inner cylinder with $R_2 = 0.5$ has center lying on $(-0.25, 0)$. The parameters U_1 and U_2 are defined for the circumferential velocities of the outer and inner cylinders, respectively. No-slip boundary conditions are specified on the fluid-solid interfaces. In this study, the outer cylinder rotates clockwise, and the inner cylinder is kept stationary ($U_1 = -1, U_2 = 0$). The velocity vector and streamline plots obtained by 270 source points are illustrated in Fig. 13. It is observed that the flow patterns are symmetric with respect to the x-axis due to the reversibility of the Stokes flow, and also a single recirculating eddy appears in the interior of the annular region. For the verification purpose, the comparison of computed velocity with the unstructured FEM result along $y = 0$ is depicted in Fig. 14. It is observed that the computed profile for 270 source points is almost indistinguishable from the FEM solution for 3000 nodes. To demonstrate further the accuracy of the present method, Table 5 shows the comparisons of net flow along $y = 0$ cross section from analytical solution [40], proposed method, and FEM with two different grids. The numerical results reveal good capability of the present method to predict Stokes flow in multi-connected domains judging from the excellent mass conservation.

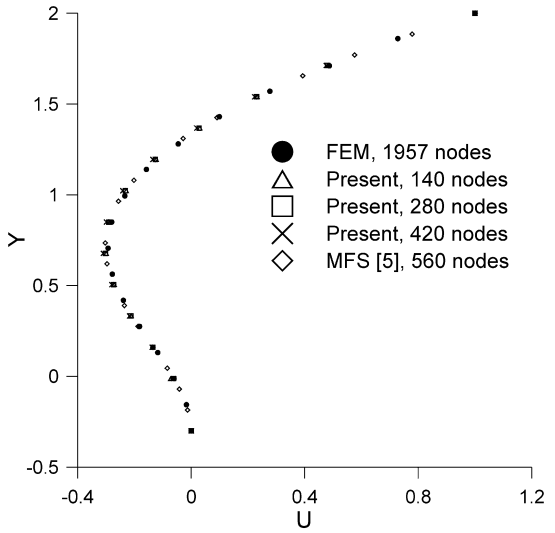

Fig. 11. Comparison of u-velocity profiles along $x = 2.5$ for a wave-shaped bottom cavity.

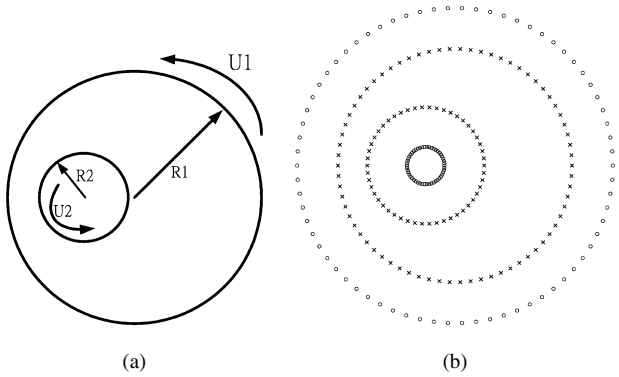

Fig. 12. (a) Schematic diagram for Stokes flow between eccentric rotating cylinders. (b) Distribution of the source (○) and field (×) points.

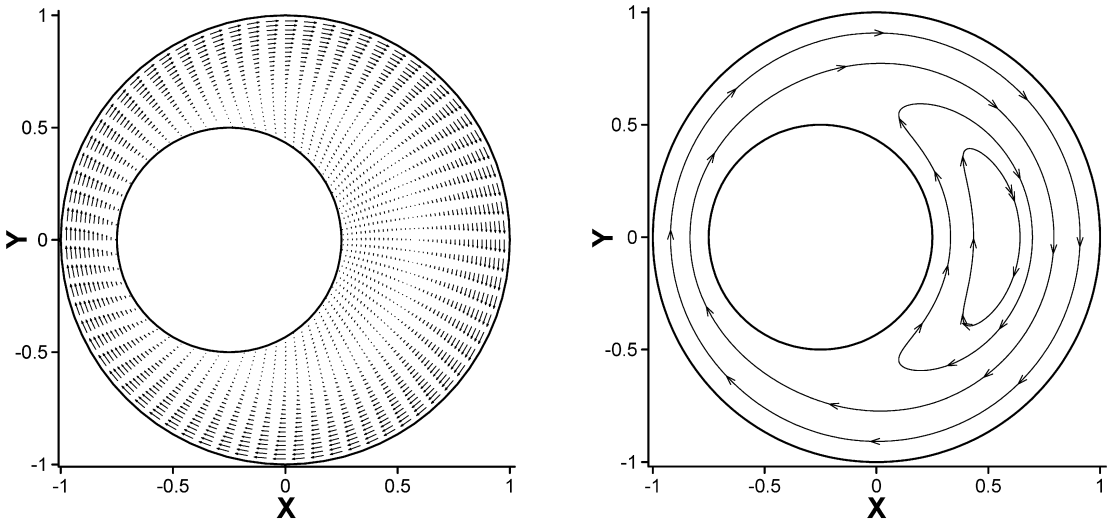

Fig. 13. (a) Velocity vectors and (b) streamlines in an eccentric rotating cylinder, $U_1 = -1$ and $U_2 = 0$ ($N = 270$).

Table 5
Comparison of the net flow in the example 4.2.4

	Analytical solution [40]	Present $N = 270$	FEM 3000 nodes	FEM 4000 nodes
Net flow $\int_{0.25}^{1} v(x,0)\,dx$	−0.17671	−0.17688	−0.17649	−0.17659
Net flow $\int_{-0.75}^{-1} v(x,0)\,dx$	0.17671	0.17706	0.17632	0.17637

4.2.3. A uniform flow passing a pair of spheres

In the last test the proposed scheme is used to simulate a uniform flow passing a pair of spheres as sketched in Fig. 15, which also shows the distribution of the source and field points. Fig. 16 depicts the velocity vector field in the plane $z = 0$ obtained by using 240 source points. There are no analytical solutions available in the literature to verify the present scheme for such a complex geometry. However, the reliability of the presented method can be judged from

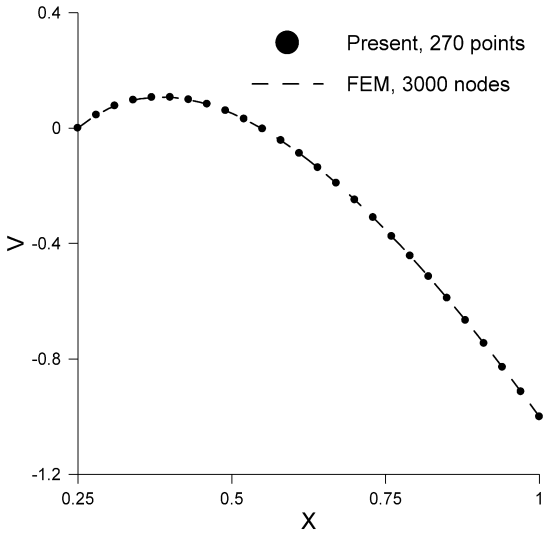

Fig. 14. Comparison of v-velocity profiles along $y = 0$ for the eccentric cylinders.

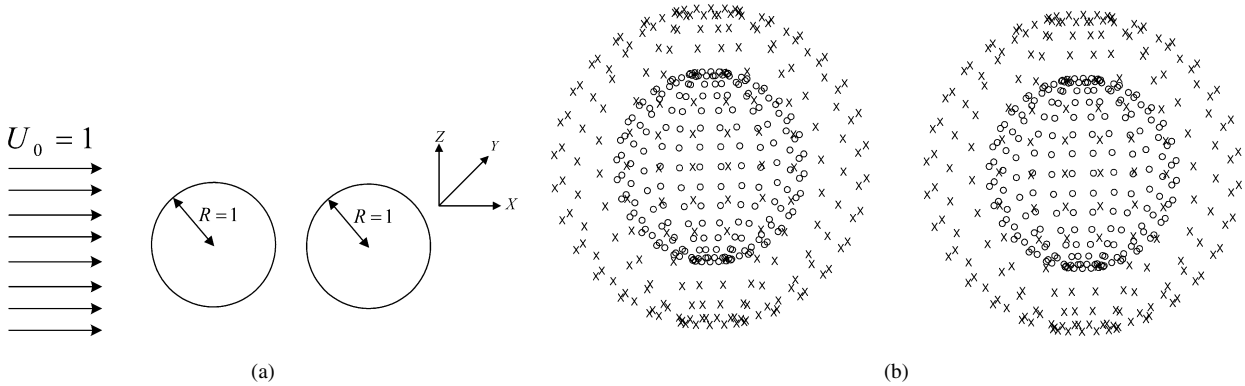

(a) (b)

Fig. 15. (a) Flow field configuration of flow passing a pair of spheres. (b) Distribution of the source (○) and field (×) points.

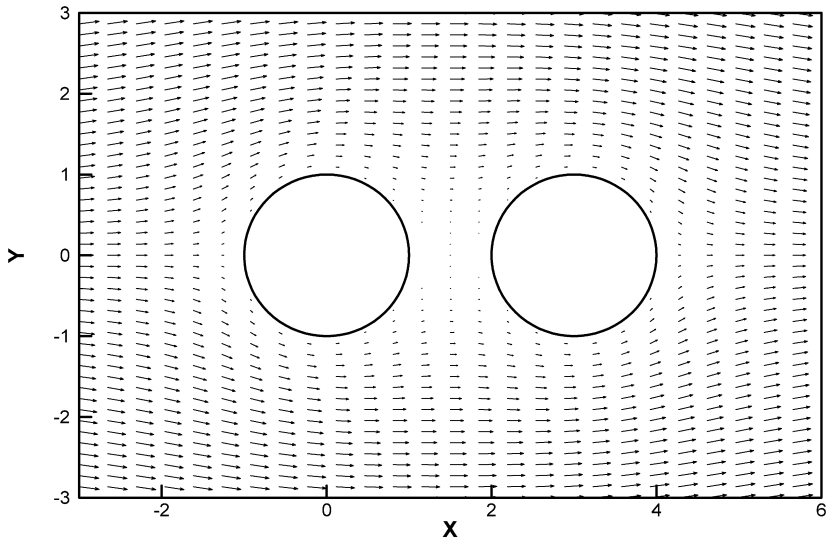

Fig. 16. Velocity vector for the Stokes flow at the plane of $z = 0$ ($N = 240$).

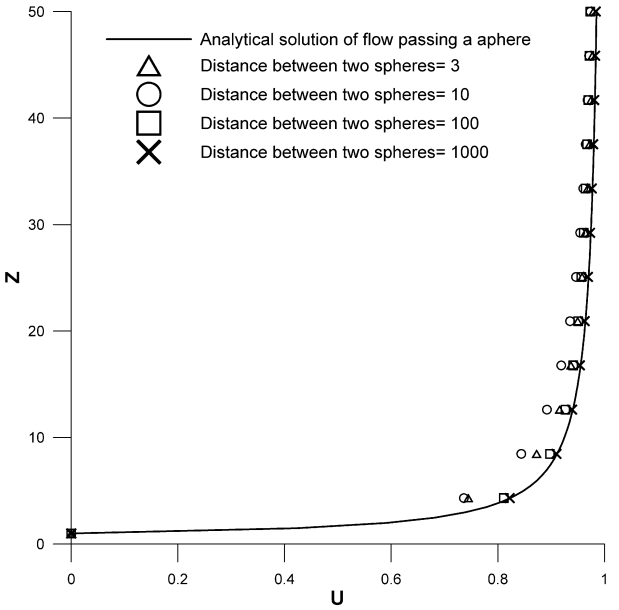

Fig. 17. u-velocity profile at the line $x = y = 0$ with different distances between two spheres ($N = 392$).

the reasonable physical characteristics. Although the presence of the sphere has effect over large distance, it always has an enough space between two spheres such that the velocity field is not interfered by another sphere. It is observed that, when the two spheres are far away from each other, the velocity distribution near one of the spheres is almost the same as that of uniform flow passing a sphere as studied in Section 4.1.2. Comparison of the velocity profiles by 392 source points in the z direction at $x = y = 0$, obtained by the other sphere located at the downstream with different distances, is depicted in Fig. 17. It took 532 points for the MFS based on the Stokeslets [7] to obtain the same accurate solutions. When the distance is one thousand times the sphere diameter, the numerical result is also indistinguishable from the analytical solution of the uniform flow passing a sphere. Therefore, it is convinced that the presented method can be easily extended to predict the uniform flow passing a pair of spheres or even more spheres with an arbitrary arrangement.

5. Conclusions

This paper uses the MFS based on the dual-potential formulation of the velocity potential and stream function vector to establish a simple, accurate and meshless numerical scheme to solve 2D and 3D Stokes problems. The key idea is to simplify the fundamental solutions of Stokes flows by the combination of the much simpler fundamental solutions of Laplace and bi-harmonic equations via the Helmholtz decomposition theorem. In this way, the unknown coefficients of both the velocity potential and the stream function vector are solved when the no-slip boundary conditions are imposed. Comparing with velocity–vorticity and vorticity–potential formulations, the present algorithm considers only four instead of six variables in 3D domain, and only two instead of three variables in 2D domain in the velocity–vorticity form. There is also no need to cope with the Poisson equations if zero dilation is assumed, thus, this algorithm yields a purely boundary-type meshless method. Meanwhile, with the advantage of easy implementation for 3D problems, the employed method can be regarded as a general stream function vector formulation for Stokes problems.

This proposed numerical scheme is applied to the following five examples, for 2D problems: (1) a circular cavity, (2) a wave-shaped bottom cavity and (3) a circular cavity with the eccentric rotating cylinder; and for 3D problems: (4) a uniform flow passing a sphere and (5) a uniform flow passing a pair of spheres. Comparing with solutions of analytical and numerical schemes such as BEM, FEM and other MFS based on the Stokeslets and velocity–vorticity forms, these numerical experiments demonstrate that the present scheme is accurate by using fewer collocation points. The numerical results really show good capability of the MFS even for 2D interior Stokes flows in multi-connected

domains and 3D exterior Stokes problems with single or multiple bodies of structures. As a result the proposed meshless method could offer a simple alternative to other numerical methods with or without mesh generation and can be applied to industrial Stokes flows.

Acknowledgements

The National Science Council of Taiwan is gratefully appreciated for providing the financial support for this research work under the Grant No. NSC 93-2611-E-002-001. We are also grateful to the associate editor and two anonymous referees for their constructive comments.

References

[1] Y. Abousleiman, A.H.-D. Cheng, Boundary element solution for steady and unsteady Stokes flow, Comput. Methods Appl. Mech. Engrg. 117 (1994) 1–13.
[2] A. Zeb, L. Elliott, D.B. Ingham, D. Lesnic, The boundary element method for the solution of Stokes equations in two-dimensional domain, Eng. Anal. Bound. Elem. 22 (1998) 317–327.
[3] C.J.S. Alves, A.L. Silvestre, Density results using Stokeslets and a method of fundamental solutions for the Stokes equations, Eng. Anal. Bound. Elem. 28 (2004) 1245–1252.
[4] D.L. Young, C.W. Chen, C.M. Fan, K. Murugesan, C.C. Tsai, Method of fundamental solutions for Stokes flows in a rectangular cavity with cylinders, Eur. J. Mech. B Fluids 24 (2005) 703–716.
[5] D.L. Young, S.J. Jane, C.M. Fan, K. Murugesan, C.C. Tsai, The method of fundamental solutions for 2D and 3D Stokes problems, J. Comput. Phys. 211 (2006) 1–8.
[6] C.W. Chen, D.L. Young, C.C. Tsai, K. Murugesan, The method of fundamental solutions for inverse 2D Stokes problems, Comput. Mech. 37 (2005) 2–14.
[7] C.C. Tsai, D.L. Young, D.C. Lo, T.K. Wong, Method of fundamental solutions for three-dimensional Stokes flow in exterior field, J. Engrg. Mech. ASCE 132 (2006) 317–326.
[8] C.M. Fan, D.L. Young, Analysis of the 2D Stokes flows by the non-singular boundary integral equation method, Int. Math. J. 2 (2002) 1199–1215.
[9] D.L. Young, S.C. Jane, C.Y. Lin, C.L. Chiu, K.C. Chen, Solutions of 2D and 3D Stokes laws using multiquadrics method, Eng. Anal. Bound. Elem. 28 (2004) 1233–1243.
[10] C.C. Tsai, D.L. Young, A.H.-D. Cheng, Meshless BEM for three-dimensional Stokes flows, CMES 3 (2002) 117–128.
[11] A. Karageorghis, G. Fairweather, The method of fundamental solutions for the numerical solution of the biharmonic equation, J. Comput. Phys. 69 (1987) 434–459.
[12] A. Karageorghis, G. Fairweather, The Almansi method of fundamental solutions for solving biharmonic problems, Int. J. Numer. Methods Engrg. 26 (1988) 1668–1682.
[13] Y.S. Smyrlis, A. Karageorghis, Some aspects of the method of fundamental solutions for certain biharmonic problems, CMES 4 (2003) 535–550.
[14] A.M. Elshabka, T.J. Chung, Numerical solution of three-dimensional stream function vector components of vorticity transport equations, Comput. Methods Appl. Mech. Engrg. 170 (1999) 131–153.
[15] C. Pozrikidis, Boundary Integral and Singularity Methods for Linearized Viscous Flow, Cambridge University Press, New York, 1992.
[16] G.J. Hirasaki, J.D. Hellums, Boundary conditions on the vector and scalar potentials in viscous three-dimensional hydrodynamics, Quart. Appl. Math. 28 (1970) 293–296.
[17] A.T. Chwang, T.Y.-T. Wu, Hydromechanics of low-Reynolds-number flow. Part. 2. Singularity method for Stokes flow, J. Fluid Mech. 67 (1975) 787–815.
[18] T. Dabros, A singularity method for calculating hydrodynamic forces and particle velocities in low-Reynolds-number flows, J. Fluid Mech. 156 (1985) 1–21.
[19] V.D. Kupradze, M.A. Aleksidze, The method of functional equations for the approximate solution of certain boundary value problem, USSR Comput. Math. Math. Phys. 4 (1964) 82–126.
[20] M.A. Golberg, The method of fundamental solutions for Poisson's equations, Eng. Anal. Bound. Elem. 16 (1995) 205–213.
[21] K. Balakrishnan, P.A. Ramachandran, Osculatory interpolation in the method of fundamental solutions for nonlinear Poisson problems, J. Comput. Phys. 172 (2001) 1–18.
[22] C.S. Chen, M.A. Golberg, Y.C. Hon, The method of fundamental solutions and quasi-Monte Carlo method for diffusion equations, Int. J. Numer. Methods Engrg. 43 (1998) 1421–1436.
[23] D.L. Young, C.C. Tsai, K. Murugesan, C.M. Fan, C.W. Chen, Time-dependent fundamental solutions for homogeneous diffusion problems, Eng. Anal. Bound. Elem. 28 (2004) 1463–1473.
[24] A. Karageorghis, The method of fundamental solutions for the calculation of the eigenvalues of the Helmholtz equation, Appl. Math. Lett. 14 (2001) 837–842.
[25] D.L. Young, S.P. Hu, C.W. Chen, C.M. Fan, K. Murugesan, Analysis of elliptical waveguides by the method of fundamental solutions, Micro. Opt. Tech. Lett. 44 (2005) 552–558.

[26] M. Katsurada, H. Okamoto, A mathematical study of the charge simulation method. I, J. Fac. Sci. Univ. Tokyo Sect. IA Math. 35 (1988) 507–518.
[27] T. Kitagawa, Asymptotic stability of the fundamental solution method, J. Comput. Appl. Math. 38 (1991) 263–269.
[28] Y.S. Smyrlis, A. Karageorghis, Numerical analysis of the MFS for certain harmonic problems, Math. Model. Numer. Anal. 28 (2004) 495–517.
[29] G. Fairweather, A. Karageorghis, The method of fundamental solutions for elliptic boundary value problems, Adv. Comput. Math. 9 (1998) 69–95.
[30] M.A. Golberg, C.S. Chen, The method of fundamental solutions for potential, Helmholtz and diffusion problems, in: M.A. Golberg (Ed.), Boundary Integral Methods: Numerical and Mathematical Aspects, WIT Press/Computational Mechanics Publications, Boston, 1999, p. 103.
[31] H.A. Cho, M.A. Golberg, A.S. Muleshkov, X. Li, Trefftz method for time dependent partial differential equations, Comput. Mat. Cont. 1 (2004) 1–37.
[32] C.W. Chen, C.M. Fan, D.L. Young, K. Murugesan, C.C. Tsai, Eigenanalysis for membranes with stringers using the methods of fundamental solutions and domain decomposition, CMES 8 (2005) 29–44.
[33] W.F. Ames, Numerical Methods for Partial Differential Equations, third ed., Academic Press, Boston, 1992.
[34] G. Arfken, Mathematical Methods for Physicists, third ed., Academic Press, Orlando, 1985.
[35] J.C. Tannehill, R.H. Pletcher, D.A. Anderson, Computational Fluid Mechanics and Heat Transfer, second ed., Taylor & Francis Press, Philadelphia, 1997.
[36] E. Weinan, J.G. Liu, Finite difference methods for 3D viscous incompressible flows in the vorticity–vector potential formulation on nonstaggered grids, J. Comput. Phys. 138 (1997) 57–82.
[37] T.Y. Hwu, D.L. Young, Y.Y. Chen, Chaotic advections for Stokes flow in a circular cavity, J. Engrg. Mech. ASCE 123 (1997) 774–782.
[38] D.J. Tritton, Physical Fluid Dynamics, Oxford University Press, New York, 1988.
[39] E. Guyon, J.P. Hulin, L. Petit, C.D. Mitescu, Physical Hydrodynamics, Oxford University Press, Oxford, 2001.
[40] B.Y. Ballal, R.S. Rivlin, Flow of a Newtonian fluid between eccentric rotating cylinders: inertial effects, Arch. Rational Mech. Anal. 62 (1976) 237–294.